Current induced switching in sub-micrometric perpendicular magnetic anisotropy MTJs

João Fidalgo da Silva
joao.fidalgo.da.silva@ist.utl.pt

Instituto Superior Técnico, Lisboa, Portugal

October 2018

Abstract

The spin-transfer torque effect is of great interest for magnetoresistive random access memory (MRAM) applications. Simultaneously achieving high TMR, low RA product, low critical current for switching and high thermal stability in MTJ stacks with perpendicular magnetic anisotropy relies on stack optimization. MR values increase from 20-30% to values in the order of 150% upon annealing at temperatures in the range 300^oC - 400^oC. R(H) characterization shows that an in-plane anisotropy in as deposited samples becomes an out-of-plane easy axis under annealing at intermediate temperatures of 300^oC, and may return to in-plane or become ambiguous due to FM coupling of the free and reference layers at higher temperatures. R(I) curves show different behaviours, including reversible transitions between 2 resistive states, but also intermediate stable resistance states, Barkhausen jumps and high resistance set with applied field, but not with applied current. These indicate a non-coherent magnetization reversal. Critical current densities J_c, in the order of 2×10^{10} A/m^2, show a correlation with a spacer material in the stack, having larger J_c for a Ta spacer, while no correlation with a stack buffer material is extracted. J_c values are considerably lower in the sample with a 1.4nm FL thickness, in the order of 1×10^9 A/m^2, but FM coupling of the magnetic layers leads to only a low resistance state a zero current/field.

Keywords: Spin-transfer torque, Current-induced switching, Perpendicular magnetic anisotropy, Nanofabrication, Magnetic tunnel junction

1. Introduction

1.1. Motivation and objectives

Nowadays, electronics are a dominating field of work. In fact, the increase in number of silicon-based processors is exponential[1]. More specifically, the need for more electronic components in smaller areas motivates the study and development of nanoelectronic components. Spintronics has been a rewarding area with the development several types of devices, such as magnetic field sensors and magnetoresistive random access memories (MRAM).

One of the main disadvantages of conventional MRAMs, where the magnetization inversion is done by an applied magnetic field (fig. 1), is the need for a high applied current for writing operations. While thermally assisted switching has been explored[2], the operation time increases due to the need for subsequent cooling of the device. In order to obtain low switching currents and low operation times, other alternatives must be explored.

The employment of current induced switching (CIS) by spin-transfer torque (STT) can lead to low write power and low write time[3]. A storage device

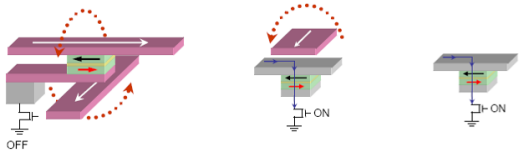

Figure 1: Comparison between MRAM architectures. Left: Conventional MRAM; Center: Thermally assisted MRAM; Right: Spin-transfer torque MRAM.

based on this functionality is referred to as STT-MRAM. In this scheme, the same electrodes that are used for reading may be used for writing, leading to simpler integration. High thermal stability (ratio between energy barrier of magnetization inversion and thermal energy) at small feature sizes can be achieved by perpendicular magnetic anisotropy (PMA) of the magnetic layers[4].

The optimization of the materials used and fabrication processes is a crucial point for obtaining reliable devices for data storage applications.

The work was developed at INESC-MN, and

the main goal was to demonstrate current-induced switching (CIS) in magnetic tunnel junctions (MTJ) with PMA, with feature sizes under 1000nm. The figures of merit are $TMR > 50\%, R \times A < 10\Omega\mu m^2, J_c < 10^6 A/cm^2$. The impact of annealing on the R(I) behaviour was also investigated.

1.2. State of the art

1.2.1 Tunneling magnetoresistance and MRAMs

Jullire measured a TMR of 14% in 1975, at a temperature of 4.2K[5]. Only in 1995 higher values of TMR were reported by Miyazaki and Tezuka[6], with 30% at 4.2K and 18% at 300K in Fe/GeO/Fe junctions, and by Moodera *et al*, with 24% at 4.2K and 11.8% at 295K, in CoFe/Al_2O_3/Co junctions[7]. These structures were used for HDD (hard disk drive) read heads starting in 2004, by Seagate, and have been employed for this ever since.

The highest reported TMR value at room temperature of 604% was obtained in 2008 by Ikeda *et al*, with CoFeB/MgO/CoFeB junctions[8]. However, for full engineered stacks, where layers with other specific functions are introduced (magnetization pinning, for instance), values of TMR are in the order of 200%[9, 10]. Junctions based on CoFeB magnetic layers have been widely studied based on the high TMR obtained.

At INESC-MN, MgO-based MTJs are explored not only for memory applications, but also for magnetic field sensor applications[11, 12]. In 2014, a two-step annealing process aimed at increasing MgO barrier MTJ structures linear responsivity yielded devices with sensitivities up to 0.1%/Oe[13]. More recently, the breakdown mechanisms were investigated in MgO junctions with feature sizes down to 50nm[14]. For a junction with 300nm feature size, a TMR of 123.9%, $R \times A$ of $7.0\Omega\mu m^2$ and critical switching current density of $1.4 \times 10^{10}\ A/m^2$ were obtained.

The first demonstration of a MRAM with a MTJ cell was in 1996[15]. In 1999, the first chip demonstrations based on MRAMs were done by IBM, with a capacity of 1kbit, and by Motorola, with a capacity of 512kbit. Nowadays, chips with capacities over 1Gbit and areal densities of 256Mb/cm^2, can be fabricated[1]. However, these MRAM structures are based on reversal by current-generated magnetic fields, and for small area junctions the need for high applied fields leads to high power consumption. Therefore, low write current and small area alternatives are being researched.

Tunneling through a barrier can be modeled by Simmons' model[16], assuming symmetrical electrodes:

$$I(V) = \frac{e}{2\pi h}\frac{A}{t^2}\Bigg((\phi - \frac{eV}{2})exp\Big(-\frac{4\pi t\sqrt{2m_e}}{h}(\phi - \frac{eV}{2})\Big) \tag{1}$$

$$-(\phi + \frac{eV}{2})exp\Big(-\frac{4\pi t\sqrt{2m_e}}{h}(\phi + \frac{eV}{2})\Big)\Bigg) \tag{2}$$

1.2.2 Perpendicular magnetic anisotropy

MTJ structures based on CoFeB electrodes and MgO oxide barrier have shown a record TMR of 604% with an in-plane anisotropy[8], and have therefore been explored for perpendicular anisotropy. Ikeda *et al* have shown that for small enough thickness of CoFeB, under 1.5nm, the easy axis lies out of the plane[17]. Three main anisotropy types can be found in this case: magnetocrystalline anisotropy favoring the out-of-plane configuration due to bcc crystalization of the CoFeB films after annealing, shape anisotropy favoring the in-plane configuration, and interface anisotropy, predicted to have an origin in the hybridization of the Fe 3d orbitals and the O 2p orbitals.

1.2.3 Current induced switching - Spin-transfer torque

The spin-transfer torque effect was first predicted in 1996, by Slonczewski[18], and it was reported in 2000 by Albert *et al*[19]. Various studies applying this effect for data storage in a STT-MRAM architecture, have been reported[17, 20], with several industry giants like TDK, IBM, Samsung and Micron presenting demonstrations. In 2014, TDK showed STT-MRAMs with TMR over 150% and high thermal stability ($E/K_bT = 100$) at room temperature in devices with dimensions under 40nm, with thermal stability being observed until 400^oC[21]. In 2016, IBM and Samsung focused on write error rates in STT-MRAM structures. The write error rate measures the probability that a given critical current with a given pulse width will not switch the magnetization direction, typically due to thermal fluctuations of the magnetization. They showed a write error rate of 10^{-6} in devices with dimensions ranging from 11nm to 50nm, with applied current pulses of 10ns[22]. In 2017, IBM, Samsung and Micron recurred to a double MTJ structure in order to reduce the critical current to $8\mu A$ at pulses of 10ns, with a write error rate of 10^{-9} in 11nm junctions[23]. The critical current density for switching J_c is given by, in a monodomain approach:

$$J_c = \frac{2e\alpha\mu_0 M_s H_{eff} t}{\eta\hbar} \quad (3)$$

where e is the electron charge, α is the Gilbert damping parameter, μ_0 is the vacuum permeability, M_s is the saturation magnetization, H_{eff} is the effective magnetic field, t is the free layer thickness, η is the spin polarization of the current and $\hbar$ is Planck's reduced constant.

However, if the magnetization reversal is not single domain-like, owing to domain related processes, a smaller effective volume (activation volume) can be reversed. This volume can be calculated as:

$$V_{act} = \frac{\eta\hbar I_c}{4\alpha e K_u} \quad (4)$$

where I_c is the critical current and K_u is the effective anisotropy constant.

2. Experimental details

Full pMTJ stacks, provided by an external collaboration, with the structure Si substrate/seed/ $[Co(0.5)/\ Pt(0.2)]_6$/ Co(0.6)/ Ru(0.8)/ Co(0.6)/ $[Pt(0.2)/\ Co(0.5)]_3$/ Pt(0.2)/ reference layer separation / FeCoB(1)/ MgO/ FeCoB(1.3)/ free layer enhancement / MgO/ cap (nominal thicknesses in nm) were nanofabricated into nanopillars with diameters ranging between 50nm and 1000nm at the INESC-MN cleanroom environment, by e-beam lithography (RAITH150) and ion beam etching (N3600). Samples were annealed under vacuum at different temperatures after nanofabrication, with temperature increase during 55min, and keeping the defined annealing temperature during 80min, and with no applied magnetic field.

Samples differ in free layer thickness (either 1.3nm or 1.4nm) and specific layers within the stack, that will be referred to as spacer and buffer layers (either W or Ta). Therefore, the notation for samples will be FL [thickness in nm], buffer/spacer.

Characterization methods consist of R(H) characterization by application of a perpendicular to plane field with a permanent magnet, and resistance measurement with applied current. R(H) characterization consists in the measurement of the electrical resistance, in a 4-point probe configuration, while a permanent magnet with a field of $926 \pm 28\ Oe$ at the surface center is approximated to the sample and then removed. The resistance is measured when the magnet is approximated and after it is removed, for each face (1 and 2) of the magnet. A representative curve is presented in fig. 2, where the points where each magnet face is put close to the sample and removed is indicated.

Resistance-current loop measurements were done recurring to a 4-point probe system, where the current application and voltage measurement were controlled by software. The current was applied in 500ms pulses. The current was increased from 0A to a maximum current value I_{max} and then decreased to a minimum (negative) value I_{min}, and then returned to 0. The maximum and minimum currents were increased slowly, until a significant variation of resistance was verified, to avoid dielectric breakdown of the samples at considerable currents. The current was applied from the top to the bottom electrode in all samples.

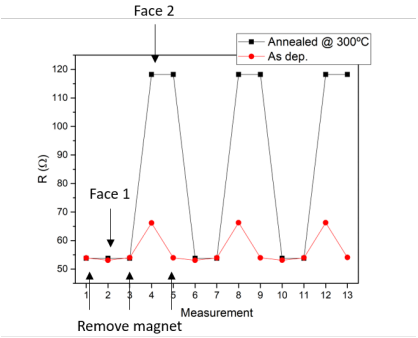

Figure 2: Example of resistance measurement with permanent magnet, showing where face 1 and face 2 are put close to the sample, as well as where the magnet is removed.

3. Results

3.1. Magnetotransport measurements

The resistance measurements with a permanent magnet are shown in fig. 3, for different annealing temperatures, for sample FL 1.3nm, W/Ta. The nanopillar nominal diameter for all measurements is 450nm.

The as deposited samples showed a behaviour consistent with an in-plane efective anisotropy, where the resistance has intermediate values between the high and low measured resistances, when the magnet is removed. This observation is consistent with previous results[24], and indicates that the interface anisotropy is not enough to achieve an out-of-plane easy axis prior to annealing. The presence of boron near the barrier hinders the interface anisotropy. The offset of this "zero-field resistance" from the average between the high and low resistances is attributed to a ferromagnetic coupling between the free and reference layers.

Upon annealing, the behaviour changes drastically. Between 300^oC and 320^oC, the behaviour is that which is expected of an MTJ with an out-of-plane easy axis, where, after the field is applied to invert the magnetization into the P/AP state and then removed, the resistance is kept low/high. The diffusion of boron away from the barrier enhances the interface anisotropy, and ultimately reorients the easy direction from the stack plane to a perpendicular axis.

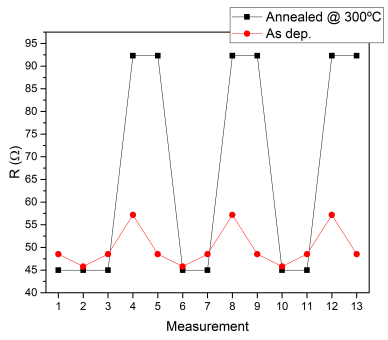

(a)

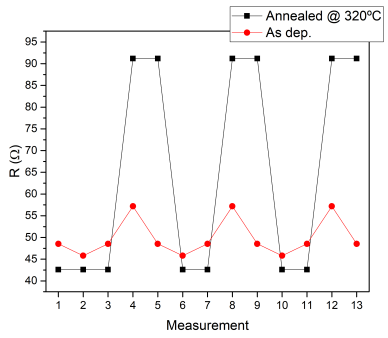

(b)

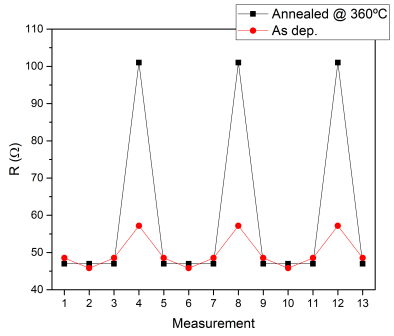

(c)

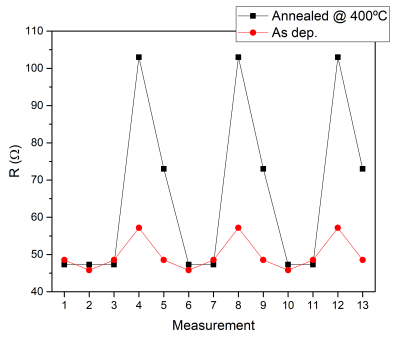

(d)

Figure 3: Resistance measurements with permanent magnet of sample 1.3nm, W/Ta, at different annealing temperatures, for a fixed nanopillar diameter of 450nm.

At 360^oC, when the magnet is removed, the resistance is the same as the low resistance, independently of whether the field was applied with face 1 or 2. This is indicative of a relatively strong ferromagnetic coupling between the free and reference layers, in the sense that it overcomes the anisotropy energy to invert the magnetization even when no magnetic field is applied. A consequence of this is that the easy direction becomes ambiguous under this characterization method.

At 400^oC, the "zero-field resistance" after applying a field in the P direction and removing it is consistent with the low/P resistance, while that measured after applying a field in the AP direction and removing it is an intermediate resistance. This does not coincide with either of the in-plane or out-of-plane cases. This indicates that the magnetization reversal is not coherent, and domain-related inversion mechanisms, such as nucleation, are dominant.

For samples FL 1.3nm, Ta/W and FL 1.4nm, W/W, similar measurements were made. For the sample FL 1.3nm, Ta/W, at annealing temperatures of 300^oC, 320^oC, 340^oC and 380^oC, a behaviour similar to that observed in sample FL 1.3nm, W/Ta at annealing temperatures of 300^oC and 320^oC, showing a perpendicular easy axis. For sample FL 1.4nm, W/W, the easy configuration is ambiguous from this type of measurement at annealing temperatures of 300^oC and 340^oC, but a behaviour similar to that observed in as deposited samples is achieved at annealing temperatures of 360^oC, indicating an easy plane configuration.

The MR is consistently increased with annealing over 300^oC, from values in the 20-30% range to $\sim$ 150%, owing to tunneling coherence achieved under MgO crystallization[25].

3.2. Current-induced switching

3.2.1 Representative R(I) curves

An example resistance measurement for sample FL 1.3nm, W/Ta, annealed at 300^oC is shown in fig. 5. For this sample, at this annealing temperature only, the resistance shown at a given current I corresponds to a measurement where the current I is applied, and then the resistance is measured with a small current of 100 μA (see fig.4). The inset values of MR and RA correspond to the values measured with the permanent magnet, and the indicated diameter is the nominal nanopillar diameter.

Step-like curves are observed, showing intermediate stable resistance states between those measured with the permanent magnet. These are reminiscent of Barkhausen jumps[26], where local defects affect the magnetization inversion locally. The activation volume was calculated for these curves with eq. 4, using the current applied to set a high resistance and the current applied to set the lowest

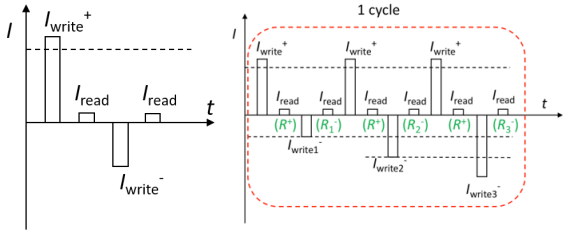

(a) (b)

Figure 4: Measurement method for resistance states (pulse width=500ms). Left: measurement method for resistance state at given current; Right: cycle for measurement of all resistance states for a given sample.

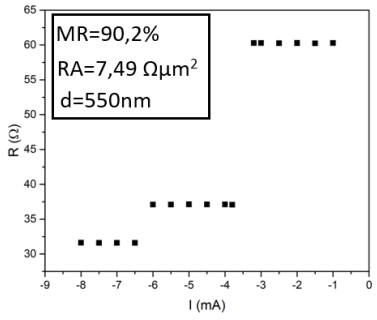

(a)

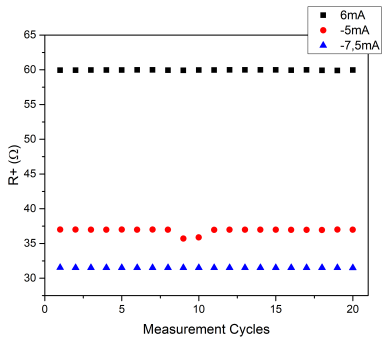

(b)

Figure 5: Resistance states for nanopillar of sample w/ FL 1.3nm, W/Ta, annealed at 300^oC, with nominal diameter of 500nm. Top: Resistance measured at small current after given current is applied; Bottom: Resistance measurements at small current after applying current indicated in legend.

resistance, and an effective anisotropy constant of 0.21 MJ/m^3[17], $\alpha = 0.01$ and $\eta = 0.5$, while effective volumes are calculated from the effective diameter, resulting from RA values measured after the nanofabrication.

Activation volumes are estimated to be smaller than the effective volume in these nanopillars, pointing to a subvolume activation.

R(I) curves for samples annealed at 320^oC show a consistent behaviour. A representative curve is shown in fig. 6.

The sample is put in a high resistance state with the permanent magnet. When the magnet is removed, the resistance is measured to be in the AP state. When the current is increased, the resistance decreases slowly, due to the tunneling effect, until it drops to a low resistance state, consistent with the P state resistance previously measured with the permanent magnet. When the current is further increased, a resistance increase is observed, expected to be a P to AP resistance switching. Decreasing of the current shows a decrease of the resistance back to the P state resistance, and further decreasing of the current into negative values and return to zero current does not affect the resistance significantly. Putting the opposite face of the magnet close to the sample, removing it and then measuring the same current values, the resistance was observed to coincide with the low resistance branch.

The sample was put under a high magnetic field of $1T$, or 800 kA/m (permanent magnet from annealing setup), in the perpendicular direction, in both "up" and "down" directions, and then the resistance-current loop was measured in the same conditions. Similar results were observed.

Two representative R(I) curves for samples with FL 1.3nm, Ta/W, annealed at 300^oC are shown in fig. 7.

In the top curve, a similar behaviour to that observed in sample FL 1.3nm, W/Ta at an annealing temperature of 320^oC is shown. In the bottom curve, clear switching with applied current between high and low resistances is observed, with switching from a low to high resistance at positive currents and a switching from high to low resistance at negative currents, in agreement with the expectations within a single domain-like magnetization reversal assumption.

Comparing the two curves, one can observe that the behaviour is comparable in the sense that a switching from a high to low resistance is observed at negative currents, as well as a switching from low to high resistance at positive currents.

For comparison, a curve from a previously measured sample, with a FL with 1.3nm thickness, and buffer/spacer of W/W, annealed after stack deposition at 400^oC, is shown in fig. 8.

Nom. diameter	Effective volume	Activation volume
700 nm	$6.8\times10^{-22}\ m^3 6$	$4.44\times10^{-22}\ m^3$
550 nm	$4.58\times10^{-22}\ m^3$	$2.39\times10^{-22}\ m^3$
500 nm	$3.92\times10^{-22}\ m^3$	$2.83\times10^{-22}\ m^3$

Table 1: Estimated activation volumes for nanopillars with FL 1.3nm, W/Ta, annealed at 300^oC, compared with effective volumes.

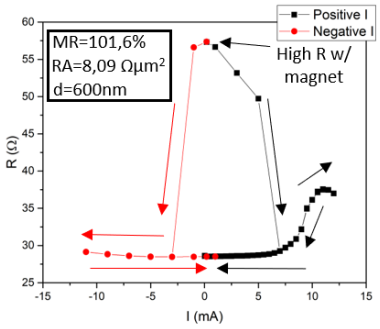

Figure 6: Example R(I) curve of sample w/ FL 1.3nm, W/Ta, annealed at 320^oC.

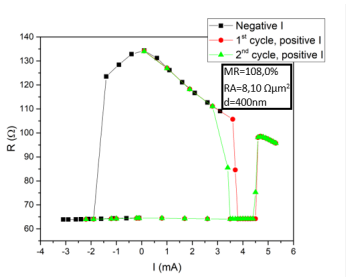

(a)

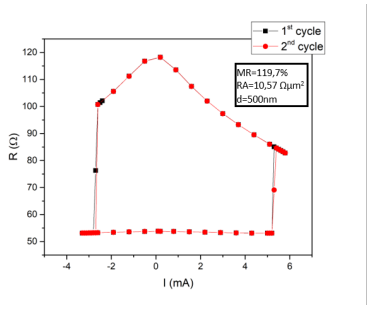

(b)

Figure 7: Example curves of sample w/ FL 1.3nm, Ta/W, annealed at 300^oC.

Clear switching from high to low and low to high resistance is observed, with only two resistance states. In this ideal case, a single domain-like approach explains the observed result, with the magnetization being in the parallel and anti-parallel configurations for low/high resistance states respectively, and a steep switching being observed between the two states, characteristic of coherent magnetization reversal.

3.2.2 Critical current/current density results

Two critical current values are taken, when possible, from the obtained R(I) curves: an I_-, corresponding to a transition from a high to a low resistance when the current is decreased, and an I_+, corresponding to a transition from a low resistance to a high resistance when the current is increased. When the transition is not imediate, the average value is taken, and the ambiguity of the value is taken into account in the experimental error. Fig. 9 indicates the I_- and I_+ in representative curves.

To remove the FM coupling contribution, the measured critical current is calculated as:

$$I_c = \frac{I_+ - I_-}{2} \tag{5}$$

The calculated I_c values for samples FL 1.3nm, W/Ta and FL 1.3nm, Ta/W are shown in fig. 10. For sample 8, critical current values could only be calculated for an annealing temperature of 300^oC, and therefore are only compared later with other samples.

Note that the measured critical current values increase with increasing nanopillar diameter, as was expected for a constant critical current density.

The comparison of the critical current density between different spacer/buffer materials and between 1.3nm and 1.4nm FL thicknesses is done in fig. 11. The annealing temperature is fixed as 300^oC, with the exception of the sample FL 1.3nm, W/W, that was annealed post-deposition at 400^oC.

J_c values in the order of $2\times10^{10}\ A/m^2$ are obtained. Comparing with state-of-the-art values for CoFeB/MgO/CoFeB PMA junctions[17], where values in the order of $10^9\ A/m^2$ are reported, higher critical current densities are generally observed. This is related to the pillar dimensions being larger than those usually studied for STT applications. The dynamics are dominated by domain movement and non-coherent rotation, where processes are always irreversible.

Although the sample FL 1.3nm, W/W was annealed at 400^oC while the others were annealed at 300^oC, a correlation is observed between the critical current density J_c and the spacer. For a spacer of Ta, the J_c values are generally larger than for

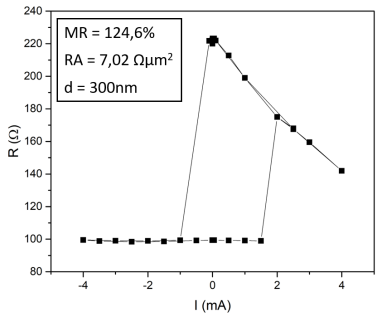

Figure 8: R(I) curve measured for sample w/ FL 1.3nm, W/W, annealed post deposition at 400^oC.

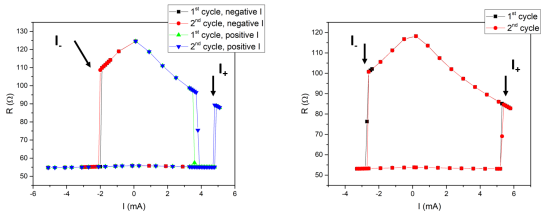

(a) (b)

Figure 9: I_- and I_+ values indicated in representative curves.

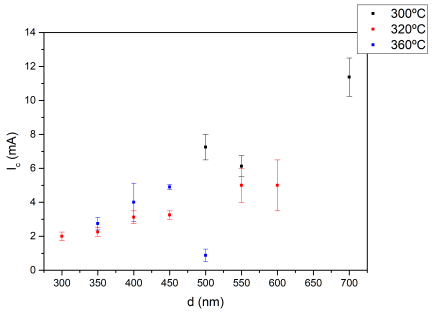

(a)

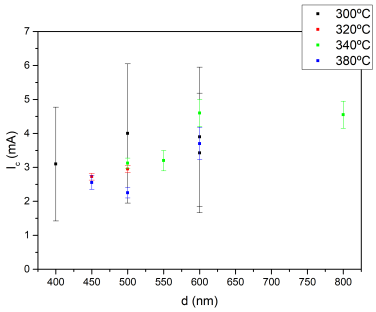

(b)

Figure 10: Calculated I_c values from R(I) measurements of sample w/ FL 1.3nm, W/Ta (top) and Ta/W (bottom), for the tested annealing temperatures.

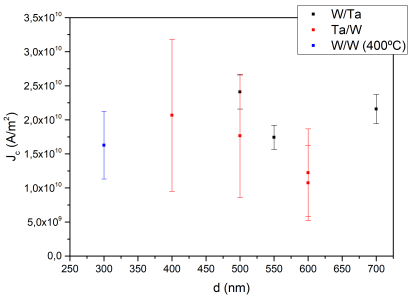

(a)

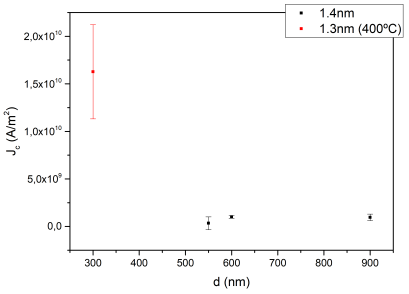

(b)

Figure 11: Critical current density J_c calculated from R(I) measurements, as a function of buffer/spacer structure (top) and of free layer thickness (bottom).

a spacer of W, possibly owing to enhanced PMA. No particular correlation is observed between the J_c values and the buffer material.

For a FL thickness of 1.4nm, the measured J_c values are significantly smaller. The expected result was either a smaller critical current or an in-plane easy configuration, owing to the smaller interface PMA.

4. Conclusions

R(H) characterization of as deposited samples shows an in-plane configuration, while annealing at temperatures over 300^oC increase MR from 20-30% to $\sim 150\%$ and an out of plane axis is observed for sample FL 1.3nm, Ta/W at annealing temperatures of 300^oC and 320^oC, and for sample FL 1.3nm, W/Ta at all tested annealing temperatures. The crystallization of MgO leads to coherent tunneling and high MR, while the diffusion of boron away from the junction enhances the PMA.

R(I) curves measured show complex behaviours, comprising clear and reversible low-high and high-low resistance switching, but also multiple stable resistance states, resistive transitions with Barkhausen jumps, and remanent high resistance state with applied perpendicular magnetic field but not with applied current. An estimation of an activation volume from measurements, when compared with the effective volume of the free layer, indicates sub-volume activation, providing evidence towards non-coherent magnetization reversal mechanisms.

Calculated critical current densities J_c are in the order of $2 \times 10^{10}\ A/m^2$ indicate a correlation with the spacer material, where the critical current density is generally larger for a Ta spacer than for a W spacer. The FL thickness decreases the critical current density, to values in the order of $1 \times 10^9\ A/m^2$, but the R(I) curve offset is large when compared to these currents. The results are attributed to a FL thickness near the spin reorientation transition, effectively showing in-plane effective anisotropy at higher annealing temperatures of 360^oC.

Acknowledgements

I would like to acknowledge my supervisors, Prof. Susana Freitas and Dr. Ana Silva, as well as Hua LV and Prof. Diana Leito.

References

[1] A. Hirohata and K. Takanashi. Future perspectives for spintronic devices. *Journal of Physics D: Applied Physics*, 47(19):193001–193040, 2014.

[2] I. L. Prejbeanu, M. Kerekes, R. Sousa, H. Sibuet, O. Redon, B. Dieny, and J. Nozires. Thermally assisted MRAM. *Journal of Physics: Condensed Matter*, 19(16):165218, 2007.

[3] J. W. Lu, E. Chen, M. Kabir, M. R. Stan, and S. A. Wolf. Spintronics technology: past, present and future. *International Materials Reviews*, 61(7):456–472, 2016.

[4] S. Ikeda, H. Sato, M. Yamanouchi, H. Gan, K. Miura, S. Kanai, S. Fukami, F. Matsukura, N. Kasai, and H. Ohno. Recent progress of perpendicular anisotropy magnetic tunnel junctions for nonvolatile VLSI. *SPIN*, 2(3):1240003, 2012.

[5] M. Jullire. Tunneling between ferromagnetic films. *Physics Letters A*, 54(3):225–226, 1975.

[6] T. Miyazaki and N. Tezuka. Giant magnetic tunneling effect in Fe/Al2O3/Fe junction. *Journal of Magnetism and Magnetic Materials*, 139(3):L231–L234, 1995.

[7] J. Moodera, L. Kinder, T. Wong, and R. Meservey. Large magnetoresistance at room temperature in ferromagnetic thin film tunnel junctions. *Physical Review Letters*, 74(16):3273–3276, 1995.

[8] S. Ikeda, J. Hayakawa, Y. Asjizawa, Y. Lee, K. Miura, H. Hasegawa, M. Tsunoda, F. Matsukura, and H. Ohno. Tunnel magnetoresistance of 604% at 300K by suppression of Ta diffusion in CoFeB/MgO/CoFeB pseudo-spin-valves annealed at high temperature. *Applied Physics Letters*, 93(8):82508, 2008.

[9] D. Leitao, A. Silva, E. Paz, R. Ferreira, S. Cardoso, and P. Freitas. Magnetoresistive nanosensors: controlling magnetism at the nanoscale. *Nanotechnology*, 27(4):045501, 2015.

[10] D. Watanabe, M. Oogane, S. Mizukami, Y. Ando, and T. Miyazaki. Boron composition dependence of spin-transfer switching in magnetic tunnel junctions with CoFeB free layers. *Japanese Journal of Applied Physics*, 48(1):013001, 2009.

[11] J. Cao, Y. Liu, Y. Ren, F. Wei, and P. Freitas. Effect of annealing temperature on formation of superparamagnetism in CoFeB/MgO/CoFeB magnetic tunnel junctions. *Applied Surface Science*, 314:443–446, 2014.

[12] S. Cardoso, C. Cavaco, R. Ferreira, L. Pereira, M. Rickart, P. Freitas, N. Franco, J. Gouveia, and N. Barradas. Characterization of CoFeB electrodes for tunnel junctions. *Journal of Applied Physics*, 97(10):10C916, 2005.

[13] D. Leito, A. Silva, R. Ferreira, E. Paz, F. Deepack, S. Cardoso, and P. Freitas. Linear nanometric tunnel junction sensors with exchange pinned sensing layer. *Journal of Applied Physics*, 115(17):17E526, 2014.

[14] H. Lv, D. Leito, Z. Hou, P. Freitas, S. Cardoso, T. Kmpfe, J. Mller, J. Langer, and J. Wrona. Barrier breakdown mechanism in nano-scale perpendicular magnetic tunnel junctions with ultrathin MgO barrier. *AIP Advances*, 8(5):55908, 2018.

[15] Z. Wang and Y. Nakamura. Spin tunneling random access memory (STRAM). *IEEE Transactions on Magnetics*, 32(5):4022–4024, 1996.

[16] J. Simmons. Generalized formula for the electric tunnel effect between similar electrodes separated by a thin insulating film. *Journal of Applied Physics*, 34(6):1793–1803, 1963.

[17] S. Ikeda, K Miura, H. Yamamoto, K. Mizunuma, H. Gan, M. Endo, S. Kanai, J. Hayakawa, F. Matsukura, and H. Ohno. A perpendicular-anisotropy CoFeBMgO magnetic tunnel junction. *Nature Materials*, 9(9):721–724, 2010.

[18] J. Slonczewski. Current-driven excitation of magnetic multilayers. *Journal of Magnetism and Magnetic Materials*, 159(1-2):L1–L7, 1996.

[19] F. Albert, J. Katine, R. Buhrman, and D. Ralph. Spin-polarized current switching of a Co thin film nanomagnet. *Applied Physics Letters*, 77(23):3809–3811, 2000.

[20] J. Hayakawa, S. Ikeda, Y. Lee, R. Sasaki, T. Meguro, F. Matsukura, H. Takahashi, and H. Ohno. Current-driven magnetization switching in CoFeB/MgO/CoFeB magnetic tunnel junctions. *Japanese Journal of Applied Physics*, 44(41):L1267–L1270, 2005.

[21] L. Thomas, G. Jan, J. Zhu, H Liu, Y. Lee, S. Le, R. Tong, K. Pi, Y. Wang, D. Shen, R. He, J. Haq, J. Teng, V. Lam, K. Huang, T. Zhong, T. Torng, and P. Wang. Perpendicular spin transfer torque magnetic random access memories with high spin torque efficiency and thermal stability for embedded applications (invited). *Journal of Applied Physics*, 115(17):172615, 2014.

[22] J. Nowak, R. Robertazzi, J. Sun, G. Hu, J. Park, J. Lee, A. Annunziata, G. Lauer, R. Kothandaraman, E. O'Sullivan, P. Trouilloud, Y. Kim, and D. Worledge. Dependence of voltage and size on write error rates in spin-transfer torque magnetic random-access memory. *IEEE Magnetic Letters*, 7:1–4, 2016.

[23] G. Hu, J. Nowak, G. Lauer, J. Lee, J. Sun, J. Harms, A. Annunziata, S. Brown, W. Chen, Y. Kim, N. Marchack, S. Murthy, C. Kothandaraman, E. O'Sullivan, J. Park, M. Reuter, R. Robertazzi, P. Trouilloud, Y. Zhu, and D. Worledge. Low-current spin transfer torque MRAM. In *2017 International Symposium on VLSI Design, Automation and Test (VLSI-DAT)*, 2017.

[24] Y. Liu, L. Hao, and J. Cao. Effect of annealing conditions on the perpendicular magnetic anisotropy of Ta/CoFeB/MgO multilayers. *AIP Advances*, 6(4):045008, 2016.

[25] S. Yuasa and D. Djayaprawira. Giant tunnel magnetoresistance in magnetic tunnel junctions with a crystalline MgO(001) barrier. *Journal of Physics D: Applied Physics*, 40(21):R337–R354, 2007.

[26] A. Timopheev, B. Teixeira, R. Sousa, S. Aufret, T. Nguyen, L. Buda-Prejbeanu, M. Chshiev, N. Sobolev, and B. Dieny. Inhomogeneous free layer in perpendicular magnetic tunnel junctions and its impact on the effective anisotropies and spin transfer torque switching efficiency. *Physical Review B*, 96(1):014412, 2017.